Geomechanics for Energy and the Environment 40 (2024) 100614

Contents lists available at ScienceDirect

Geomechanics for Energy and the Environment

journal homepage: www.elsevier.com/locate/gete

Influence of mechanical strength on gas migration through bentonite: Numerical analysis from laboratory to field scale

Jung-Tae Kim [a], Changsoo Lee [a,*], Minhyeong Lee [a], Jin-Seop Kim [a], E. Tamayo-Mas [b], J.F. Harrington [b]

[a] Korea Atomic Energy Research Institute (KAERI), 111, Daedeok-daero, 989beon-gil, Yuseong-gu, Daejeon, 34057, Republic of Korea
[b] British Geological Survey (BGS), Keyworth, Nottingham, United Kingdom

ARTICLE INFO

Editors-in-Chief:
Professor Lyesse Laloui and Professor Tomasz Hueckel

Keywords:
Gas migration
Bentonite
Dilatancy-controlled gas flow
Damage model
Preferential pathway

ABSTRACT

Understanding the gas movement phenomenon within the deep geological repository is essential for assessing the disposal system's long-term stability. The primary gas transport mechanism through the bentonite is dilatancy-controlled flow, which differs from gas flow in general porous media. This flow is characterized by gas movement through microcracks created under relatively high gas pressure conditions, and the intrinsic permeability, air-entry pressure, and mechanical strength of the medium change due to the generation and propagation of these microcracks. Therefore, dilatancy-controlled flow cannot be simulated using the classical two-phase flow modeling technique. This study constructed the H^2MD (two-phase hydraulic-mechanical-damage) numerical model by combining a damage model to simulate material degradation and the resulting change in intrinsic permeability with a classical two-phase flow model. In addition, the numerical model was tested against a 1D laboratory gas injection test investing gas flow mechanisms in the buffer, and a sensitivity analysis was performed on tensile strength, a key factor in the damage model for gas movement phenomenon. In the validation study, the proposed model successfully simulated the key features observed in the test: rapid stress and pressure increase trends, changes in intrinsic permeability due to damage, and the resulting flow rate. In addition, the effect of heterogeneity on the strength characteristics of each material and interfaces between materials was analyzed through field-scale test simulations, and the applicability of the model to upscaling analysis was examined. The study of heterogeneity effects confirmed that incorporating the strength characteristics of interfaces accurately simulates the gas flow path observed in actual tests. However, the model overestimated the gas flow before the gas breakthrough and underestimated the evolution of the damaged area within the buffer. Therefore, additional research on relative permeability and mechanical constitutive models is needed to improve the reliability of the current model.

1. Introduction

A deep geological repository (DGR) is considered one of the most promising methods for isolating high-level radioactive waste from human habitation.[1–4] The repository comprises a multi-barrier system of the engineered barrier system (EBS) and the natural barrier system (NBS). In particular, EBS consists of a disposal canister, buffers, and backfill materials. The buffer plays a vital role in isolating the disposal canister from the surroundings and delaying the movement of radionuclides into the environment if leakage occurs. Bentonite is the most promising material for buffers due to its low permeability and diffusion coefficients, swelling characteristics, and high sorption capacity.[5–9]

In a high-temperature and high-pressure disposal environment, gases (such as H_2, Rn, CO_2, and CH_4) may be generated due to anaerobic corrosion of the canister, water radiolysis, and microbial degradation.[1,7,10] Thus, understanding the flow of these gases among EBS components is essential for assessing the long-term stability of the repository. Marschall et al[11] defined four types of gas flow mechanism: (1) advective–diffusive transport of dissolved gas, (2) visco-capillary two-phase flow, (3) dilatancy-controlled gas flow and (4) gas transport along macro-fractures. These gas transfer mechanisms depend on the rate of gas generation. When the gas generation rate is lower than the diffusion rate, most gases dissolve into the water and transfer with diffusion or advective flow.[12] However, when the gas generation rate exceeds the diffusion rate, gas can be trapped in the pores, increasing its gas pressure. If the increased gas pressure reaches the air-entry pressure of the bentonite, visco-capillary two-phase flow may occur.[1] However, in low permeability materials, such as a bentonite-based EBS,

* Corresponding author.
E-mail address: leecs@kaeri.re.kr (C. Lee).

https://doi.org/10.1016/j.gete.2024.100614
Received 10 July 2024; Received in revised form 3 October 2024; Accepted 11 October 2024
Available online 28 November 2024

the air entry pressure can be very high, limiting gas flow through visco-capillary flow. When the gas pressure reaches a critical pressure, causing physical damage to the bentonite, microcracks develop inside the EBS, forming a preferential path and causing dilatancy-controlled gas flow. These microcracks can develop into macro-fractures.[13–15]

Marschall et al[11] described the dilatancy-controlled flow as the dominant gas transport mechanism through bentonite, wherein gas flow is facilitated by microcracks formed under specific stress conditions. The gas migration through the microcracks leads to alterations in the pore structure and an increase in pore space, which subsequently increases the intrinsic permeability of the buffer and changes the capillary pressure and water retention relationship, contributing to the formation of preferential pathways. This feature of dilatancy-controlled flow has also been observed and proven through experimental studies. Various laboratory-scale gas injection tests have been conducted, and the following features have been observed from tests: (1) increasing gas pressure at the injection filter during the constant gas inflow phase, (2) observation of rapid increases in stress and pressure appearing above a certain gas pressure, and (3) rapid increases in inflow and outflow gas rates. These characteristics are evidence of a breakthrough, rapid gas movement due to the formation of a preferential path after the creation of microcracks due to high gas pressure.[14,16,17] Additionally, similar features were observed in the field-scale gas injection test (Lasgit) performed by Cuss et al.[18,19]

However, the formation of these pathways and the resulting gas movement through them have a very complex mechanism. Hence, ongoing research is being conducted to identify its key features. In many studies, an approach to simulate the preferential pathway was used by applying a model that considers mechanical effects on intrinsic permeability, directly affecting gas flow and pressure evolution. These models include a gas pressure-based model derived from the experimental observations,[20,21] a porosity-based model that considers the effect of pore volume changes,[22,23] a strain-based model that considers the impact of pore structure changes,[24] and a damage model that considers both changes in mechanical and hydraulic properties.[25,26] In particular, DECOVALEX, an international joint research project that develops and verifies numerical models to identify phenomena related to such multiphysics complex behavior, has conducted research to identify gas movement phenomena in the buffer in two stages (DECOVALEX-2019 Task A, DECOVALEX-2023 Task B). Participants developed and verified their models using laboratory- and field-scale test data provided by the task lead.[23,27]

In particular, the hydraulic-mechanical-damage coupled modeling technique, which applies a damage model that considers both mechanical deterioration and hydraulic characteristics of the medium, is being used by many researchers as well as within DECOVALEX-2019 Task A and DECOVEALEX-2023 Task B to simulate dilatancy-controlled flow in bentonite. Fall et al[25] introduced a hydraulic-mechanical-damage modeling technique using Tang's damage model. Xue et al[28] studied the effect of the lateral pressure coefficient on the evolution of the damaged area. Dagher et al[29] analyzed the impact of modeling the damaged zone propagation and the resulting gas migration phenomenon according to various stress–strain constitutive models (i.e., linear elastic, elastoplastic, and non-local elastoplastic). In these comparisons, for one-dimensional laboratory gas injection test simulations, the linear elastic medium assumption combined with the damage model best matched experimental data. Yang and Fall[30] proposed the damage model simulating micro to macroscopic cracks and analyzed the damage area evolution according to initial damage, microstructure size, and strain rate. The literature review indicates that the damage model based on elastic behavior is straightforward yet effectively simulates dilatancy-controlled flow in bentonite. Consequently, this study aims to model dilatancy-controlled flow by applying a damage model rooted in the elastic behavior of bentonite. Despite the reliance of the damage model on the strength characteristics of the buffer, there is a notable paucity of studies examining its impact on these characteristics.

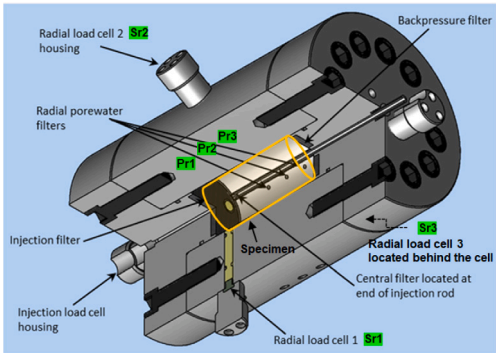

Fig. 1. Test apparatus for 1D gas injection test.
Source: Modified from Daniels and Harrington.[31]

Moreover, the damage model encompasses several uncertain variables, including residual tensile strength and ultimate tensile strain.[15]

In this study, a H^{2}MD coupled numerical model to simulate dilatancy-controlled gas flow in bentonite is developed based on the linear elastic constitutive relation with the damage model. A modified damage model, which reduces uncertain variables such as residual tensile strength and ultimate tensile strain, has been proposed, and the numerical model is tested against laboratory-scale gas injection test results. In this process, a sensitivity analysis is performed on the tensile strength of bentonite to analyze the impact of strength characteristics on damage zone propagation, stress and pressure response, and flow rate simulation. In addition, the strategy is tested against field scale test data to analyze the effect on gas movement when tensile strength is applied as material (component) heterogeneity. The applicability of upscaling techniques is also examined.

2. One-dimensional gas injection test

In this section, we concisely describe the one-dimensional (1D) gas injection test, a validation test for the numerical model developed in this study. The 1D gas injection test, conducted by Daniels and Harrington,[31] used a rigid cell designed to maintain a constant volume even under high pressure. The cell was equipped with five load cells and five pressure gauges strategically positioned to capture stress and pressure variations at different locations within the sample, as depicted in Fig. 1 (Note: In Fig. 1, the legends of the stress and pressure sensors utilized to indicate the results of the numerical model are highlighted in green). The dimension and physical properties of the pre-compacted Mx80 bentonite block used in this study are summarized in Table 1.

The test is divided into three phases: (1) a hydration phase, (2) a gas injection phase, and (3) a ceasing gas injection phase. This section describes some features that can be observed at each phase based on the test data provided by the Task lead. Comprehensive details on the test equipment and methodologies are described in previous studies.[16,31]

In the hydration phase, the sample is saturated by injecting water using a syringe pump through stainless steel filters (including injection, backpressure, and radial surface filters depicted in Fig. 1). This phase corresponds to the time interval from the start of the test to approximately 40 days, see Fig. 2. Of paramount importance during this phase is the observation of stress distribution. As illustrated in Fig. 2(a), stress levels exhibit an initial increase upon commencement of water injection, followed by convergence to a stable state. This means that the bentonite block is fully saturated, and also swelling is complete. The hydration phase ends when the stress convergence is being observed. The converged stress value is generally considered to be the swelling pressure of compacted bentonite.[23,31]

Then, the gas injection phase takes place. A noteworthy feature of this phase is the abrupt increases in stress and pressure, evident in

Table 1
Material properties for one-dimensional gas injection test[31].

Sample	Length [mm]	Diameter [mm]	Water content [–]	Dry density [kg/m^3]	Porosity [–]	Saturation [–]
Mx80	119.90	59.69	0.266	1.579	0.430	97.8

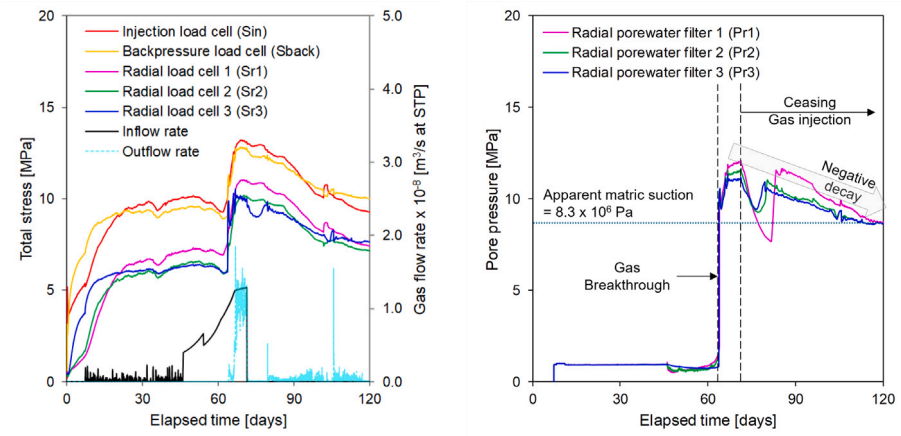

(a) Evolution of Total Stress and Gas Flow Rate Over Time (b) Evolution of pore pressure

Fig. 2. Test data for 1D gas injection test offered by Task lead.

both Figs. 2(a) and 2(b). Initially, the stress and pressure variations are not observed even through the gas injection (40–63 days in Fig. 2). However, approximately 63.8 days from the beginning of the test, rapid increases in stress and pressure are observed. This phenomenon aligns with the characteristic manifestation of gas breakthrough. The sudden surge in gas outflow rate indicated the formation of a preferential pathway within the bentonite block, facilitating rapid gas migration (Fig. 2(a)).

The final step is when gas ceases. In this test, gas injection was stopped after a steady-state flow between gas inflow and outflow was observed following the gas breakthrough phenomenon, which occurred at approximately 71 days. Upon cessation of gas injection, both stress and pressure gradually declined and showed a tendency towards convergence. The pressure value at which this convergence occurs, referred to as the shut-in pressure (apparent matric suction in Fig. 2(b)), represents the minimum pressure at which gas pathways remain open. This shut-in pressure is significant as it can be used to define the air-entry value for the sample in subsequent numerical analyses.[32]

3. H^{2}MD coupled modeling approach

This section describes the approach for mathematically modeling the gas injection test previously described. The dominant physical phenomenon in this test is the dilatancy-controlled gas flow. We first need to model the two-phase flow within a porous medium to simulate this phenomenon. This flow can be numerically modeled based on mass and momentum conservation laws, given that the test is conducted under isothermal conditions, excluding energy conservation. We incorporated constitutive relations, such as Darcy's law, the water retention curve, and the damage model, to simulate key observations from the test, including gas breakthrough and the formation of preferential pathways.

3.1. Governing equations

3.1.1. Conservation of mass

In this study, we considered saturated bentonite as a porous medium with a single pore structure. As aforementioned, the mechanisms for gas transport in saturated bentonite include diffusion/advection of dissolved gases, viscous capillary two-phase flow, and transport through preferential pathways. Olivella and Alonso[33] proposed mass balance equations that account for gas transport mechanisms in all cases. But Nagra (National Cooperative for the Disposal of Radioactive Waste) reported that dissolved gases' diffusion/advection rate is negligible compared to gas migration by the other two mechanisms.[34] In addition, in the one-dimensional gas injection experiment results presented in Section 2, a substantial amount of gas was injected (inflow rate, Fig. 2(a)) before the occurrence of gas breakthrough (63 days), yet no outflow was detected during this period. However, a significant outflow (outflow rate, Fig. 2(a)) was clearly observed following the gas breakthrough. Thus, this study applied the following simplified mass balance equation for each component, α (Eq. (1)), which does not consider the diffusion/advection of dissolved gas as used in the previous study.[15]

$$\rho_\alpha \phi \left(\frac{S_\alpha}{K_\alpha} - \frac{\partial S_e}{\partial p_c} \right) \frac{\partial p_\alpha}{\partial t} + \nabla \cdot (\rho_\alpha \mathbf{q}_\alpha) = -\phi \rho_\alpha \frac{\partial S_e}{\partial p_c} \frac{\partial p_{\alpha'}}{\partial t} - S_\alpha \rho_\alpha \frac{\epsilon_v}{\partial t} \tag{1}$$

where subscript, α represents w (water) and g (generated gas, Helium in this study), respectively. ρ_α is the phase density [kg/m^3], ϕ is the porosity [–], S_α is the phase saturation [–], K_α is the bulk modulus of fluid component α [Pa], S_e is the effective saturation [–], p_c is the capillary pressure [Pa], $\mathbf{q}_\alpha$ is the Darcy's velocity of the fluid component α [m/s], ϵ_v is the volumetric strain [–], and α' denotes the fluid component other than component α.

3.1.2. Conservation of momentum

This study assumed that saturated bentonite is a mixture of solids and fluids and behaves elastically. The stress–strain relationship of the mixture porous medium conforms to Hooke's Law. The mechanical response was modeled by employing the classical equation of linear momentum conservation, expressed as follows:

$$\nabla \cdot \boldsymbol{\sigma} + \rho_m \mathbf{g} = 0 \tag{2}$$

where $\boldsymbol{\sigma}$ is the total stress tensor (positive for tension) [Pa], ρ_m is the density of the mixture [kg/m^3] expressed as

$$\rho_m = (1 - \phi)\rho_s + \phi(S_w \rho_w + S_g \rho_g) \tag{3}$$

where ρ_s, ρ_w, and ρ_g are the density [kg/m^3] of solid grain, water, and gas, respectively. To consider hydraulic-mechanical coupling effects

according to gas injection, the effective stress model (Eq. (4)) based on Biot's theory was substituted into Eq. (2).

$$\boldsymbol{\sigma} = \boldsymbol{\sigma}' + \alpha p_p \mathbf{I} \tag{4}$$

where $\boldsymbol{\sigma}'$ is the effective stress [Pa], α is the Biot's coefficient [–], p_p is the average pore pressure [Pa], and $\mathbf{I}$ is the identity tensor. The average pore pressure is defined as[27]:

$$p_p = max(p_w, p_g) \tag{5}$$

where p_w and p_g are water and gas pressure [Pa], respectively. This approach can be intuitively applied to both single-phase and two-phase flow analyses. It assumes that the larger partial pressure of each phase predominantly influences the mechanical behavior of the particles surrounding the pores.[35]

3.2. Constitutive relations

3.2.1. Hydraulic behavior

The key phenomenon in modeling the gas injection test is the movement of water and gas. This study assumed that two-phase flow is only governed by the visco-capillary two-phase flow in porous media, which can be expressed by Dary's law as follows:

$$\mathbf{q}_{\boldsymbol{\alpha}} = -\frac{\mathbf{k}_{int} k_{r\alpha}}{\mu_\alpha} \nabla(p_\alpha - \rho_\alpha \mathbf{g}) \tag{6}$$

where $\mathbf{k}_{int}$ is the intrinsic permeability [m^2], $k_{r\alpha}$ is the relative permeability of the fluid component α, μ_α is the dynamic viscosity [Pa s], p_α is the pore pressure of each fluid component [Pa], ρ_α is the phase density [kg/m^3], and $\mathbf{g}$ is the gravitational vector [m^2/s].

In the unsaturated porous media, the phase flow is governed by the intrinsic and relative permeability. The intrinsic permeability is a material property, and the relative permeability is a state property. The relative permeability is governed by the effective saturation. The effective saturation varies with the capillary pressure, and the relation between effective saturation and capillary pressure can be expressed by the van Genuchten model[36]:

$$S_e = \left[1 + \left(\frac{p_c}{p_{entry}}\right)^n\right]^{-m} \tag{7}$$

where S_e is the effective saturation of the water phase [–], p_c is the capillary pressure [Pa], p_{entry} is the air-entry pressure [Pa], m and n are shape parameters, and $n = 1/(1-m)$.

The air-entry pressure is an important factor in the gas flow phenomenon in porous media. This depends on the pore distribution of the porous medium and is characterized by a very high value in media with very small pores, such as pre-compacted bentonite. In the gas injection test, the pore structure changes depending on the gas injection; this effect was considered by the following relationship[33]:

$$p_{entry} = p_{entry,i}\left(\frac{k_{int,i}}{k_{int}}\right)^{1/3} \tag{8}$$

where $p_{entry,i}$ is the initial air-entry pressure [Pa], $k_{int,i}$ and k_{int} are the initial intrinsic permeability and intrinsic permeability corresponding to the current-time step [m^2], respectively. The intrinsic permeability corresponding to the current-time step is described in the damage model section in detail.

The capillary pressure can be defined by

$$p_c = p_g - p_w \tag{9}$$

This study used the primary variable for the numerical model as the water and gas pressure, p_w and p_g. Therefore, the saturation of each phase (i.e., S_w, S_g) at each time step can be calculated by the following relations:

$$S_e = \frac{S_w - S_{rw}}{1 - S_{rw}} \tag{10}$$

$$S_w = S_e(1 - S_{rw}) + S_{rw} \tag{11}$$

$$S_g = 1 - S_w \tag{12}$$

where S_{rw} is the residual water saturation [–].

This study used the power law model (PLM) proposed by Mualem[37] for the relative permeability model. The model assumed that water is continuously distributed throughout the porous medium, whereas gas exists only inside the pore. Due to these assumptions, the relative permeability of gas, a non-wetting fluid, is derived to be smaller than the relative permeability of water in the relatively high effective saturation range.[15] However, in our model, when the PLM was applied as is, the gas relative permeability derived excessively small, and a numerical convergence problem occurred. Therefore, we used a modified equation for gas relative permeability as follows:

$$k_{r\alpha} = \begin{cases} k_{rw}(S_e) = S_e^{\lambda_{cap}}, & \text{for water phase} \\ k_{rg}(S_e) = 1 - S_e^{\lambda_{cap}} = 1 - k_{rw}, & \text{for gas phase} \end{cases} \tag{13}$$

where λ_{cap} is a parameter depending on the soil type.

3.2.2. Damage behavior

The most characteristic feature observed in gas injection tests is gas breakthrough, which is a phenomenon related to the rapid migration of gas. Previous studies revealed that micro-fractures within the bentonite block occurred when the gas pressure reaches the sum of the total stress (the minimum principal total stress) and tensile strength. These micro-fractures deteriorate the mechanical strength and form a preferential pathway.[1,17] To consider the deterioration of the mechanical strength, the damage model proposed by Tang et al[38] was applied in various studies.[23,25,26] This model derives the damage factor based on the strain rate, and Young's Modulus can be expressed as a function of the damage factor as follows:

$$E(D) = (1 - D)E_i \tag{14}$$

where D is the damage factor [–] and E_i is the initial Young's modulus [Pa]. The following relationship for the damage factor is here used:

$$D = \begin{cases} 0, & \text{for } \epsilon_3 < \epsilon_{t0} \\ 1 - \frac{f_{tr}}{E_0 \epsilon_3}, & \text{for } \epsilon_{t0} \le \epsilon_3 < \epsilon_{tu} \\ 1, & \text{for } \epsilon_{tu} \le \epsilon_3 \end{cases} \tag{15}$$

where f_{tr} is the residual tensile strength [Pa], ϵ_3 is the minimum principal strain [m/m], ϵ_{t0} is the tensile strain when the stress tensor reaches to the tensile strength, f_t, and ϵ_{tu} is the tensile strain corresponding to a complete tensile failure. These variables can be obtained through uniaxial tensile tests conducted on samples such as rock or concrete.[38–40]

Guo and Fall[15] stated that Tang's model may have two discontinuity points in the damage factor depending on the strain value, and the residual strength of the model is a specific property of the rock, so it is not suitable for application to bentonite. Based on this, the residual strength term was removed in this study. In addition, when using the original model, ϵ_{tu} must be assumed, which creates additional uncertainty. Therefore, this study applied a modified damage model, which was also used in the previous study.[23]

$$D = \begin{cases} 0, & \text{for } \epsilon_3 < \epsilon_{t0} \\ 1, & \text{for } \epsilon_{t0} \le \epsilon_3 \end{cases} \tag{16}$$

where ϵ_{t0} can be estimated by f_t/E_0. Thus, the tensile strength (f_t) significantly affects the evolution of the damage field.

3.2.3. Hydraulic-mechanical-damage coupled effect

Gas migration in pre-compacted bentonite is a complex HM-coupled behavior. In HM-coupled numerical modeling, intrinsic permeability with mechanical variables are applied to Darcy's law to reflect the coupling effect.[15] In gas injection experiments, the mechanical behavior affecting intrinsic permeability can be divided as follows: (1) change in pore structure due to gas injection and (2) formation of micro-fracture.

The former does not cause damage to the medium, but the latter does. Thus, this study used an intrinsic permeability model, expressed as a combination of the intrinsic permeability of undamaged and damaged zones proposed by Meschke and Grasberger[41]:

$$k_{int} = k_{ud} + k_d \tag{17}$$

where k_{ud} is the intrinsic permeability for the undamaged zone [m^2], and k_d is the intrinsic permeability for the damaged zone [m^2]. For the undamaged intrinsic permeability, a function of the porosity is assumed[25]:

$$k_{ud} = k_{int,i} exp[A(\frac{\phi_t}{\phi_i} - 1)] \tag{18}$$

where $k_{int,i}$ is the initial intrinsic permeability [m^2], A is an empirical (calibration) factor [–], ϕ_t is the current porosity [–], and ϕ_i is the initial porosity. The model[25,26] derived from experimental data linking changes in permeability with mechanical damage was used for the damaged zone:

$$k_d = \frac{D}{D_{kmax}}(k_{max} - k_{ud}) \tag{19}$$

where D_{kmax} is the rock damage value that corresponds to k_{max}, k_{max} is the maximum permeability of the damaged sedimentary rock [m^2], which should be determined experimentally for the specimen.

4. Numerical modeling

4.1. Numerical simulator

This study simulated the 1D gas injection test of Section 2 using COMSOL Multiphysics software based on the finite element method (FEM). A numerical model was developed to simulate H^2M coupled processes by combining a general form partial differential equation (PDE) module with a solid mechanics module. The two-phase flow was modeled using the general form PDE module to enforce mass conservation laws, considering the pore pressures of gas and water as the dependent variables for each phase. Furthermore, the mechanical behavior of the medium was modeled using the solid mechanics module, which solves the momentum balance equation with the displacement field as the dependent variable. The compacted bentonite block was assumed to behave as a linear elastic material. A time-dependent analysis was performed, with the primary variables (p_g, p_w, and $\mathbf{u}$) for each time step computed using the Pardiso direct solver within a fully coupled scheme.

4.2. Validation study: Laboratory-scale modeling (1D gas injection test)

4.2.1. Geometry and boundary conditions

A three-dimensional cylinder with a diameter of 59.69 mm and a length of 119.50 mm was modeled, as shown in Fig. 3. The domain consists of two filter domains and a bentonite domain, discretized into 3,355 tetrahedra elements. We separated the domain into two parts to facilitate the simulation of the compressive behavior of the bentonite near the injection filter. Instead, the filter domain was conducted only for mechanical analysis, not hydraulic analysis. Injected gas was simulated by a Dirichlet boundary condition with the time-dependent pressure data at the injection filter ($p_{g,inj}(t)$). The pressure evolution with time was briefly modified and applied to improve analysis stability, as shown in Fig. 4. All boundary conditions shown in Fig. 3 are summarized in Table 2.

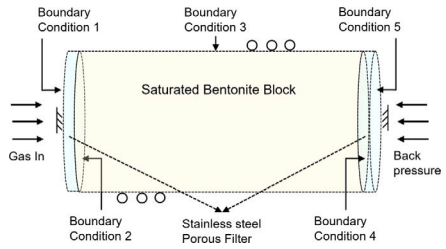

Fig. 3. Geometry and boundary conditions for 1D gas injection modeling.

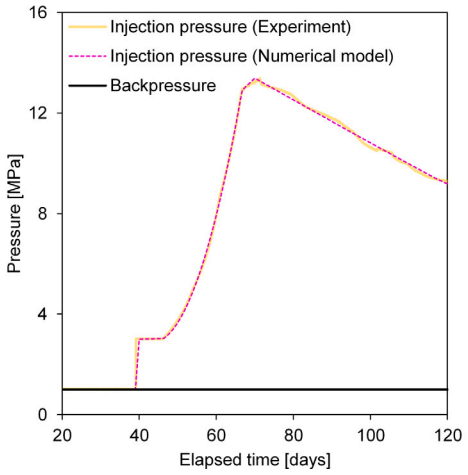

Fig. 4. Time-dependent pressure data used for gas injection modeling.

4.2.2. Material properties and calibration parameters

This section deals with input parameters and initial conditions. The material properties of bentonite were prescribed to the values provided by the task lead. In addition, the dynamic viscosity of water and gas that changes depending on temperature was assumed to be 293.15 K in the laboratory, and helium gas was assumed to follow the ideal gas equation. The hydraulic properties were prescribed by referring to the literature.[23] We needed to assume the parameters that are applied to the damage model. However, there are limitations in using all factors as calibration parameters, so literature values were used for some factors. This study selected the tensile strength, a key variable in the damage model, as a calibration parameter and conducted sensitivity analysis using it. The initial conditions were estimated and applied according to the assumptions regarding the definition of the average pore pressure of the model based on the experimental conditions. The input parameters used in this study are summarized in Table 3.

4.2.3. Modeling results

This section summarizes the sensitivity analysis results with tensile strength specified as the calibration parameter. Tensile strength was selected from 0.4 MPa to 1.4 MPa, as shown in Table 3, based on the literature value of 1 MPa.[29] Fig. 5 depicts the stress evolution of each case at the gas injection filter. The tendency for stress to increase varies depending on tensile strength. However, there was no significant difference in maximum stress in all cases. Except for the case where the tensile strength was 0.4 MPa, the stress increased linearly after the gas injection stage (40 days after the start of the test). Afterward, a rapid stress increase was confirmed at a specific point in each case. This is consistent with the stress behavior at the breakthrough moment shown in the test. The case that predicted the breakthrough timing most similar to the validation test was the case where the tensile strength was 1.2 MPa. For all cases, the developed model successfully simulated the overall trend of rapid stress changes and the maximum stress observed

Table 2
Boundary conditions for the 1D gas injection test.

Boundary No.	Adjacent domain	Physics	BCs for mass conservation	BCs for momentum conservation
1	Injection filter	Mechanical	–	Fixed
2	Injection filter, Bentonite	Hydraulic	Dirichlet BC: $p_g = p_{g,inj}(t),\ p_w = p_{w,i}$	–
3	Bentonite	Hydraulic & Mechanical	Zero flux	Roller
4	Outlet filter, Bentonite	Hydraulic	Dirichlet BC: $p_g = p_{g,i},\ p_w = p_{w,i}$	–
5	Outlet filter	Mechanical	–	Fixed

Table 3
Material properties used in sensitivity analysis.

	Meaning	Symbol	Unit	Value		Notes
				Bentonite	Filter	
Mechanical	Dry density of solid grain	ρ_g	kg/m^3	2700	–	
	Initial porosity	ϕ_i	–	0.44		Fixed[23]
	Initial Young's modulus	E_i	Pa	$3.07 \cdot 10^8$	$2.00 \cdot 10^{11}$	Fixed for Bentonite[23] Fixed for stainless filter (typical value)
	Biot's coefficient	α	–	0.65	–	
	Average density of porous media	ρ	kg/m^3	Variable derived from Eq. (3)	8000	
	Water density	ρ_w	kg/m^3	1000	–	
	Gas density (Helium)	ρ_g	kg/m^3	1.70	–	
	Bulk modulus of water	K_w	Pa	$2.20 \cdot 10^9$	–	
	Bulk modulus of gas (Helium)	K_g	Pa	p_g	–	
	Dynamic viscosity of water	μ_w	Pa s	$1.32 \cdot 10^{-3}$	–	$K_g = p_g$
	Dynamic viscosity of gas (Helium)	μ_g	Pa s	$1.76 \cdot 10^{-5}$	–	
Hydraulic	Initial intrinsic permeability	$\mathbf{k_{int,i}}$	m^2	$3.40 \cdot 10^{-21}$	–	Fixed[23]
	van Genuchten model parameter	m	–	0.50	–	Fixed[42]
	Residual water saturation	S_{rw}	–	0.01	–	
	Initial air-entry pressure	$p_{entry,i}$	Pa	$8.30 \cdot 10^6$	–	Fixed (apparent matric suction in Fig. 2(b))
Damage model	Tensile strength	f_t	Pa	$(0.4, 0.8, 1.0, 1.2, 1.4) \cdot 10^6$	–	Calibration parameter
	Empirical (calibration) factor for undamaged zone permeability	A	–	22.2	–	Fixed[43,44]
	Rock damage value	D_{max}	–	1.0	–	Fixed[43,44]
	Maximum permeability of the damaged sedimentary rock	k_{max}	m^2	$1.0 \cdot 10^{-19}$	–	Fixed[23]
Initial value	Initial pore water pressure	$p_{w,i}$	Pa	$-6.94 \cdot 10^5$	$-6.94 \cdot 10^5$	$P_{w,i}$, $P_{g,i}$ are incorporated in the M analysis, despite the absence of H analysis in the filter
	Initial pore gas pressure	$p_{g,i}$	Pa	$1.0 \cdot 10^6$	$1.0 \cdot 10^6$	

during the gas breakthrough phenomenon. However, the numerical model indicated that the stress decreases at the gas injection cessation stage, following the gas breakthrough, occurred somewhat more slowly than the actual experimental results.

Fig. 6 compares the measured values of stress and pressure sensors embedded at each location on the test apparatus and the predicted values of the numerical model. In the case of stress, Sr1 and Sr2 sensors showed overestimated values in all cases, and Sr3 showed underestimated values compared to the test value (Fig. 6(a)). In addition, the test results showed a rapid increase in stress after the breakthrough in all stress sensors. In contrast, the numerical results showed a relatively gradual increase from the gas injection stage. On the other hand, in the case of pressure, the predicted values of sensors (Pr1, Pr2, Pr3) at each location were underestimated in all cases (Fig. 6(b)). In addition, similar to the tendency of stress, there was a gradual upward trend compared to the test results. Since the numerical model in this study utilizes an effective stress model based on Biot's theory, it inferred that the trends of pressure and stress are derived similarly.

The pressure and stress trends over time predicted by the numerical model appear similar. However, the stress was relatively overestimated compared to the test data, and the pressure was relatively underestimated. It is related to the location of the stress and pressure sensors. The pressure sensors (Pr1, Pr2, Pr3) are located at the center of the cell compared to the stress sensors (Sr1, Sr2, Sr3), as shown in the upper right corner in Fig. 7. Fig. 7 shows the pressure distribution along the length of the cell. The pressure distributions predicted by the numerical model are shown as a solid line, and the pressures observed

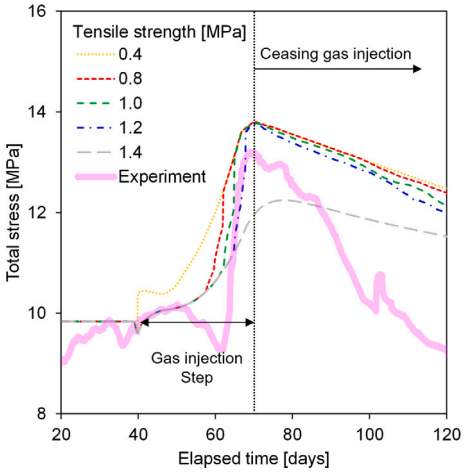

Fig. 5. Total stress evolution at the gas injection filter.

in the test are shown as marks. The predicted values result from the case where the tensile strength is 1.2 MPa. In Fig. 7, the predicted values are higher for the pressure at the points located at Pr1 to Pr3 before the breakthrough rather than the test-measured values, but the test-measured values are higher than the predicted values after the

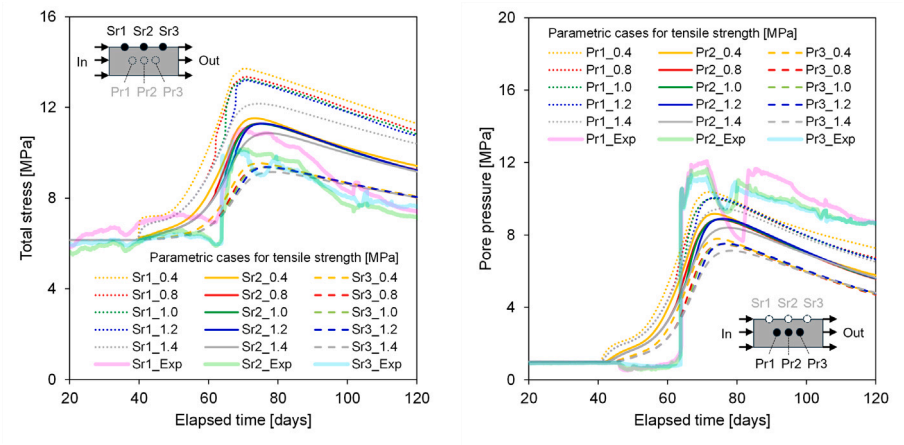

(a) Total stress evolution (b) Pore pressure evolution

Fig. 6. Comparisons between numerical modeling and experimental data.

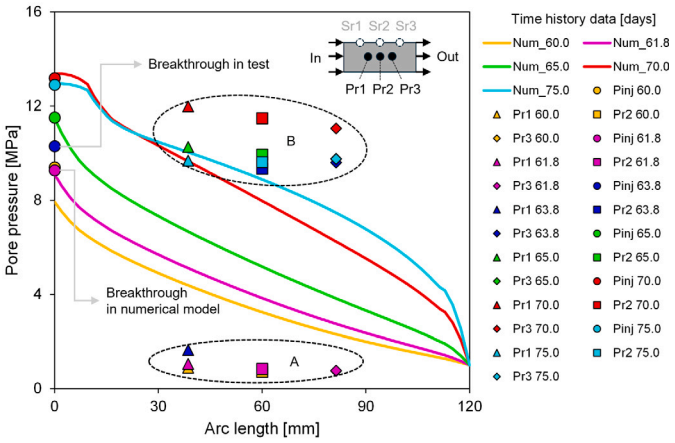

Fig. 7. Pressure evolution comparisons between numerical and test results.

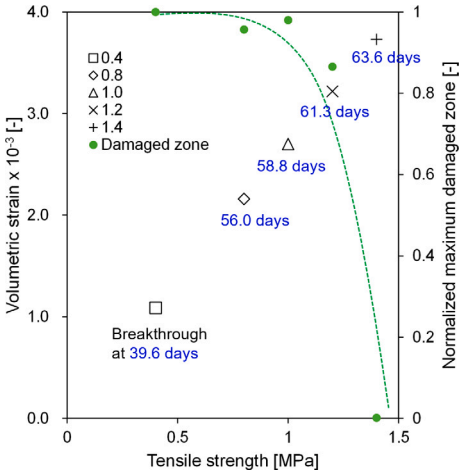

Fig. 8. Breakthrough timing and damaged area with tensile strength.

breakthrough. This is because of whether pressure propagates or not before the breakthrough. In the numerical model, gradual propagation of gas pressure occurred even before the breakthrough occurred. In contrast, the pressures were maintained at a low-pressure level measured in the test before the breakthrough (shown as section A in Fig. 7), and then a rapid increase in pressure was observed after the breakthrough (shown as section B in Fig. 7).

The difference in pressure distribution can be interpreted in two ways. The first is due to the relative permeability model (Eq. (13)), modified due to analysis convergence issues. The modified model tends to overestimate the relative gas permeability compared to the model presented by Mualem.[37] This difference induced our model to simulate excessive propagation of gas pressure into the compacted bentonite from the beginning of gas injection. The second is the effect of the damaged area. Fig. 8 shows the breakthrough timing according to tensile strength and the volumetric strain at the breakthrough moment. It also shows the normalized maximum damage area regarding the 0.4 MPa case where the maximum damage area occurred. It shows that as the tensile strength increases, the bentonite can withstand failure even at a significant strain rate, and the point at which breakthrough occurs is also delayed.

Fig. 9 shows the maximum damaged area in each case (the time of maximum damage is different for all). The maximum damaged area depends on the tensile strength. In the case where the tensile strength is 1.2 MPa in Fig. 9, even when maximum damage occurred, no damage occurred to the area where the pressure sensors Pr1 to Pr3 are located. Thus, the numerical results did not predict a rapid increase in pressure due to the breakthrough (Fig. 7). However, the 70-day and 75-day pressure prediction trends demonstrate that the numerical model accurately simulates the rapid pressure increase and propagation resulting from the breakthrough event, effectively capturing the maximum damage extent of approximately 10 mm from the injection point, as depicted in Fig. 9. However, in actual experiments, pressure propagation is transmitted rapidly to the outlet within a short time frame, and when a crack occurs across the entire buffer, the pressure dissipates quickly. This discrepancy in the speed of pressure propagation is reflected in the differences in the stress trends observed between the experimental values after gas breakthrough and the stress predictions made by the numerical model, as illustrated in Fig. 5. In the case of the numerical model, since crack propagation did not extend to the outlet, the pressure dissipation following gas breakthrough was predicted to occur more slowly than observed experimentally.

Similarly, the variance between the measured stress and pressure sensor values distributed throughout the sample and the numerical predictions shown in Fig. 6 can also be elucidated by this phenomenon. The more rapid decrease in measured stress during the experimental phase after gas breakthrough, compared to the numerical model, is attributed to the rapid pressure dissipation resulting from the formation of cracks across the entire buffer. The similarity in the trends of

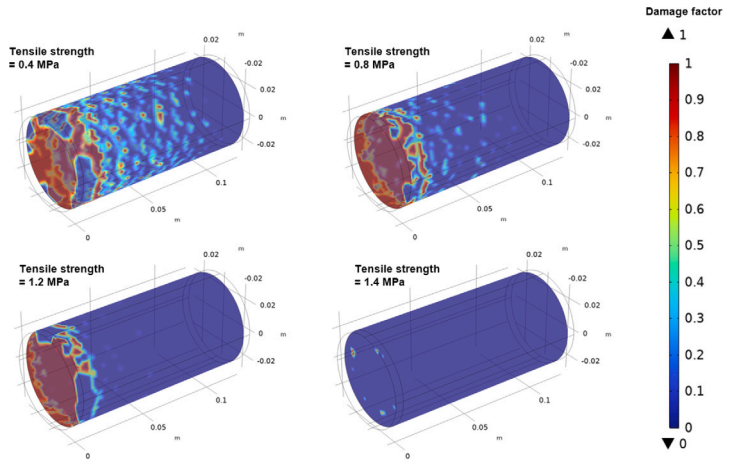

Fig. 9. The maximum damaged area with tensile strength (even though we used a modified damage model, Eq. (16), the legend appears as continuous numbers rather than 0 or 1 due to the display setting).

pressure and stress changes can be attributed to the fact that, according to Biot's theory, stress is a variable induced by pressure.

Regarding the pressure change trend, pressure at the injection filter was linearly transmitted across the sample even prior to gas breakthrough, influenced by the relative permeability model employed in the numerical simulation. Consequently, pressure reached the locations where sensors Pr1 and Pr3 are situated, but did not reflect the maximum pressure at the time of gas breakthrough. Thus, it is concluded that the numerical model predicts a pressure value post-gas breakthrough that is somewhat lower than the experimental measurement. Furthermore, the relatively smooth decrease in stress and pressure predicted by the numerical model, in contrast to the fluctuations observed in experimental measurements due to sample heterogeneity and the dynamic behavior of cracks, can be attributed to the maintained constant pressure boundary condition at the outlet, which led to pressure dissipation being predicted according to Darcy's law.

The damaged area due to the breakthrough also affects the prediction of gas inflow and outflow. Fig. 10(a) shows the gas inflow rate into compacted bentonite. In all cases (except for the extreme cases of 0.4 and 1.4 MPa), a rapid increase in inflow was predicted at the breakthrough moment. This results from reflecting the increased permeability of the damaged area due to the breakthrough through Eq. (19). In addition, the amount of gas inflow is greatly affected by the pressure gradient based on Darcy's law. In the case of 0.4 MPa, a breakthrough occurred under relatively low gas injection pressure conditions, and the gas inflow rate was predicted to be low because the pressure gradient was negligible at this time. In the case of 1.4 MPa, the damage area was tiny, so the inflow rate was low. As with the point of occurrence of breakthrough, the inflow rate was derived to be the most similar in the case of 1.2 MPa. However, the gas inflow amount before the breakthrough derived from the test could not be simulated in all cases. This is believed to be the result of the gas inflow before the breakthrough occurring not being reflected in the accumulated volume inside the inflow filter and at the bentonite interface. This effect leads to the difference between the predicted cumulative gas injection volume and the volume injected in the test, as shown in Fig. 10(b). Also, as shown in Fig. 10(c), the outflow gas rate was underestimated compared to the outflow rate observed in the test, and the total outflow gas volume (Fig. 10(d)) was accordingly underestimated in all cases. This underestimation is because the damaged area caused by the breakthrough did not spread to the outflow area, as shown in Fig. 9. This study's findings align with those reported by Dagher et al[29] The damaged zone cannot spread to the outlet because the medium is assumed to be a completely elastic body without any permanent plastic deformation. It is inferred that during gas breakthrough within a confined volume, pressure propagation leads to localized volume expansion in some regions, while compression inevitably occurs in others. This effect likely contributed to the overestimation of self-healing in the elastic media and the underestimation of the damaged area in the model predictions. It is judged that this will lead to a reduction and self-healing effect of the damaged zone. Further research is required to accurately simulate the cracks throughout the medium observed in laboratory tests. This requires modeling localized damaged zones by accounting for the heterogeneity in the material properties of bentonite.

Based on the results of the validation study, we confirmed that it effectively captures the following features observed in the test: (1) formation of a preferential path upon breakthrough due to gas injection, (2) increased permeability in the damaged area, and (3) a rapid increase in both stress and pressure. Furthermore, the sensitivity analysis of calibration parameters confirmed the influence of tensile strength within a single material on gas movement phenomena. However, this model is limited in predicting a continuous damaged area rather than a narrow, discontinuous one. To overcome these limitations, applying a constitutive model that reflects the plastic behavior of compressed bentonite or improving the model by considering the recovery effect on the hydraulic-mechanical properties of bentonite after self-healing is necessary.

4.3. Application study: Field-scale modeling (LASGIT test)

In the previous section, a laboratory-scale gas injection test was modeled to validate the applicability of the developed model for advective gas flow. Additionally, the effect of tensile strength on gas migration within homogeneous compacted bentonite was evaluated. As a result, it was confirmed that the timing of the breakthrough and the damaged area vary depending on the tensile strength. DECOVALEX-2023 Task B aimed to address several concerns that were not resolved in advective gas flow modeling in the previous phase, DECOVALEX-2019 Task A. In particular, DECOVALEX-2023 Task B aimed to evaluate the developed model's applicability for upscaling to a field-scale gas injection test.[27] Unlike laboratory-scale tests, field-scale test involves various components, including buffers, pellets, rocks, and the interfaces between these materials.

This section aims to evaluate the impact of applying material strength properties derived from laboratory-scale tests to different field-scale components on gas transfer phenomena. Specifically, the focus was on assessing the effect of considering or not considering the strength properties of the material interfaces on gas flow pathways. Additionally, we compared the actual measurements with the

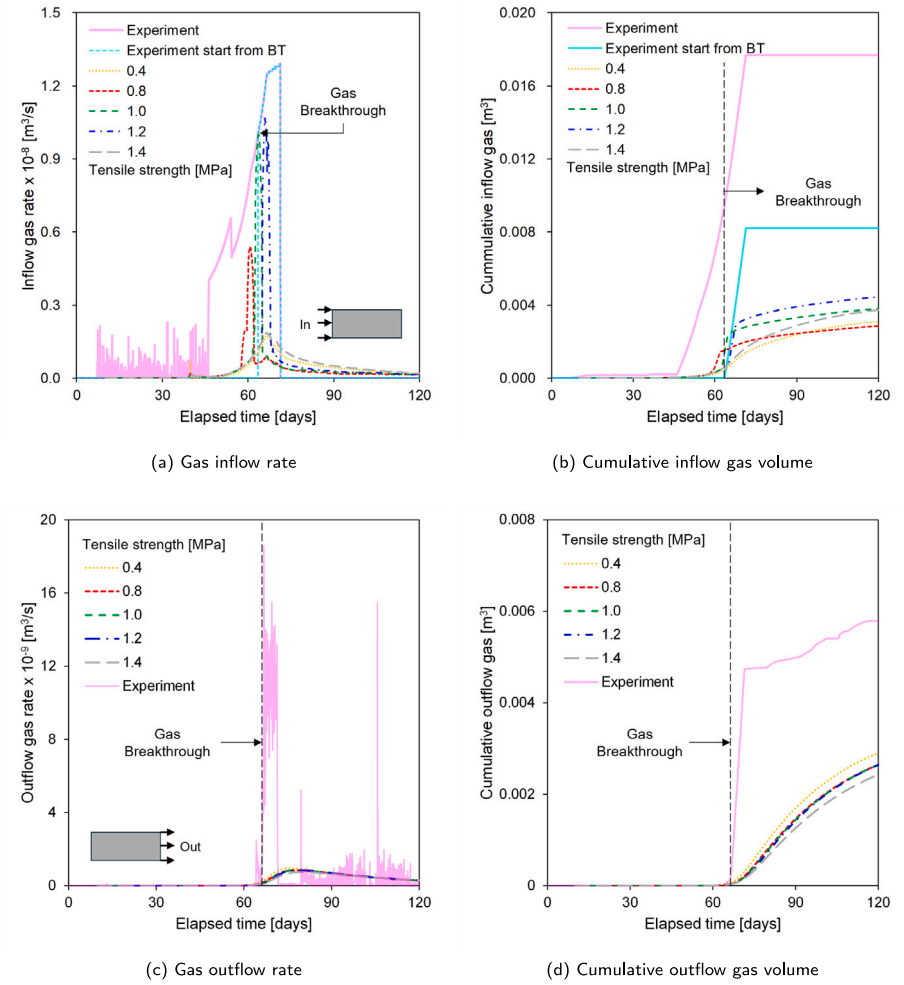

Fig. 10. Gas flow rate estimation.

numerical model predictions to evaluate the model's applicability for upscaling analysis. Despite identifying several technical limitations in the laboratory-scale simulations, the field-scale analysis was conducted to further assess the limitations of the proposed model and to inform potential improvements for future studies.

4.3.1. *Brief description of field-scale test*

The field-scale test presented in DECOVALEX-2023 Task B is Lasgit (LArge Scale Gas Injection Test), which is a gas injection test conducted by British geological survey (BGS) at a depth of 420 m in the Äspö Hard Rock Laboratory (Fig. 11). In the test, gas was injected into an engineered barrier system (EBS) consisting of multi-components such as canister, void, bentonite, pellet, and rock based on the KBS-3 concept. A field-scale EBS has been placed into a deposition hole with a length of 8.5 m and a diameter of 1.75 m. The test was conducted over approximately 15 years, starting from 2003, and involved four different gas injection tests.[18]

This study focused on the gas flow paths observed in four experiments. In all cases, gas flowed through the interface of each component (Fig. 12). Therefore, this study aimed to simulate the gas flow observed in tests by considering a multi-component system, reflecting the heterogeneity of the material. In particular, we aimed to model the fourth gas injection test, and for the efficiency of analysis, the modeling target area was selected, as shown in Fig. 12. The detailed test setup, method, and results of Lasgit are described by Cuss et al.[18]

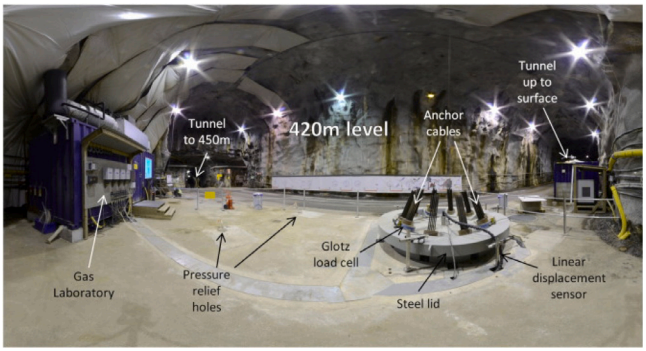

Fig. 11. A panoramic view of Lasgit test site form Cuss et al.[19]

4.3.2. *Geometry and boundary condition*

For Lasgit modeling, a three-dimensional quarter cylinder geometry consisting of 9,635 elements (hexahedral and quads) was constructed (Fig. 13(a)). The model consists of a total of four material components: bentonite (C1, R1–R4 in Fig. 13(b)), interface, pellet, and rock (Fig. 13(b)). This study assumed that two interface types (i.e., the interface between canister-bentonite and the interface between bentonite-bentonite) had the same material properties since the simulation started when both saturation and swelling phases were completed.

For mechanical analysis, a roller boundary was applied to all boundaries except the bottom boundary, where displacements were assumed

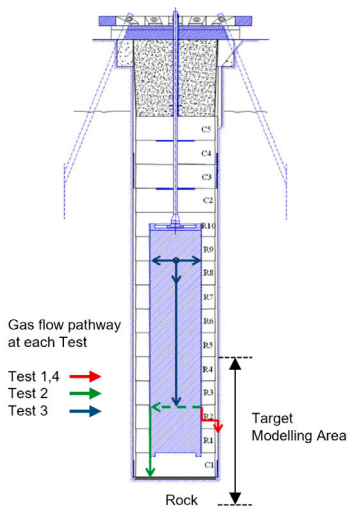

Fig. 12. Gas flow path at each test.
Source: Modified from Cuss et al.[19]

to be restrained. For hydraulic analysis, a Dirichlet boundary using the initial pore water pressure and time-dependent gas pressure data measured in the test was applied to the injection filter, and the Dirichlet boundary was applied to the initial gas and water pressures on the outer surface (Fig. 13(b)). The injection filter was modeled as a surface with an area of 0.003 m^2, shown in Fig. 13(a). Finally, the measurement values used for the comparison between the actual test and the numerical model were obtained from sensors located at four points, including two points in the R3 bentonite (PR909, UR909), where the injection filter is situated, and two points in the R1 bentonite (PR905, UR905), as shown in Fig. 13. In this context, 'PR' denotes the stress sensors, while 'UR' refers to the pore water pressure gauges.

4.3.3. Case identification and material properties

The application study aimed to simulate gas flow through the interface, as observed in the Lasgit. It was determined that this gas flow occurred because the interface's hydraulic properties differed from those of compacted bentonite. However, Villar et al[45] reported that the intrinsic permeability of the interface is not significantly different from that of intact compacted bentonite under fully saturated conditions. Based on this, we hypothesized that variations in breakthrough conditions for each component and alterations in hydraulic characteristics due to breakthrough would influence the gas flow path. To model this hypothesis, tensile strength, used as a calibration parameter in the validation study, was applied to each component to have different breakthrough conditions. Additionally, two analysis cases were selected to validate the hypothesis: one without considering interface characteristics and one with interface characteristics considered. The tensile strength assumed that the interface's tensile strength was half that of intact bentonite. Porosity and Young's modulus were estimated based on average density, and intrinsic permeability was estimated based on bentonite's average density and intrinsic permeability (provided by the task lead).[46] The input properties are summarized in Table 4.

4.3.4. Modeling results

Fig. 14 shows the propagation of the damaged zone over time for the two analysis cases (as explained in Fig. 9, the display settings result in the legend as a continuous damage factor from 0 to 1.). The occurrence and propagation of a damaged zone mean that the permeability at that location increases, which means there is a high possibility that gas will flow along this area. Analysis results considering interface characteristics show that the breakthrough occurs relatively early during gas injection. Additionally, it was confirmed that the damaged area propagated along the interface between the canister and the bentonite. This result is similar to the gas flow path observed in the Lasgit.

On the other hand, when the interface characteristics were not considered, the breakthrough occurred relatively late. And the damaged zone spreads into the buffer rather than the interfaces. After 3200 days, the damaged zone is predicted to propagate into the bentonite even when considering the interface characteristics because the pore pressure at that point in both cases is large enough to induce the breakthrough.

Rapid changes in pressure and gas saturation can be indicators of gas flow more directly than the occurrence of a damaged zone. Fig. 15 shows changes in pressure (Fig. 15(a)) and gas saturation (Fig. 15(b)) over time for the observation points (A–D) shown in Fig. 14. Here, the solid line represents an analysis that considers the interface characteristic, and the dotted line represents an analysis that does not consider the interface characteristic. The two analyses similarly predicted pressure and gas saturation for observation point A, located close to the injection filter. This is because time-dependent pressure data, a test measurement value, was applied as a Dirichlet boundary condition where the injection filter is located. On the other hand, observation points B and C change only when gas moves along the interface. At observation point D, rapid changes in pressure and saturation are observed when a breakthrough penetrating the bentonite occurs. The gradual pressure increase observed at all locations results from over-predicted pressure propagation by the modified relative permeability model (Eq. (13)), as in the results of the previous validation study.

In the case of observation points B and C, the analysis considering the interface characteristics predicted a rapid increase in pressure and gas saturation because a breakthrough occurred along the boundary from the beginning of gas injection. In contrast, the analysis that did not consider the interface characteristics predicted only a gradual increase during the early stage. On the other hand, around day 3200, when breakthroughs began to occur inside the bentonite, both analyses showed a rapid rise in pressure and gas saturation at all locations, including observation point D. In particular, the rapid pressure increase due to the breakthrough was well simulated at the observation point D, as observed in the validation study.

This study confirmed that the change in gas saturation due to gas breakthrough at all observation points, excluding the injection section, was insignificant, ranging from an initial saturation of 0.02 to a maximum of 0.069. Despite the small variation in gas saturation, the developed model well simulated the rapid change in gas saturation when the gas pressure rises rapidly (Fig. 15(b)).

Fig. 16 presents a comparison between the measured pore water pressure (Fig. 16(a)) and stress (Fig. 16(b)) data from LASGIT (provided by the task lead) and the numerical modeling results. The measured data showed initial value discrepancies at different depths due to disturbances caused during the excavation and backfilling for the installation of the test device. Therefore, for an accurate comparison, the study focused on the relative changes in values from their respective initial values over time. The numerical modeling results predicted significant changes in both stress and pore water pressure at the observation point inside the R3 bentonite, where the injection filter was located. This is attributed to the rapid pressure transmission from the injection filter, as shown in Fig. 15(a). Notably, the model predicted a rapid increase in pressure around 3,200 days, corresponding to damage initiation within the R3 bentonite. At this time, the maximum pressure change predicted by the model that did not consider the interface characteristics was larger because it predicted a wider damage zone than the model that considered the interface characteristics, as shown in Fig. 14

In contrast to the pressure data, when considering interface characteristics, the predicted stress exhibited a more pronounced change compared to the case where the interface was not considered. This discrepancy arises because the stress sensor was positioned at the boundary of the modeled geometry (Fig. 13(a)). With the consideration

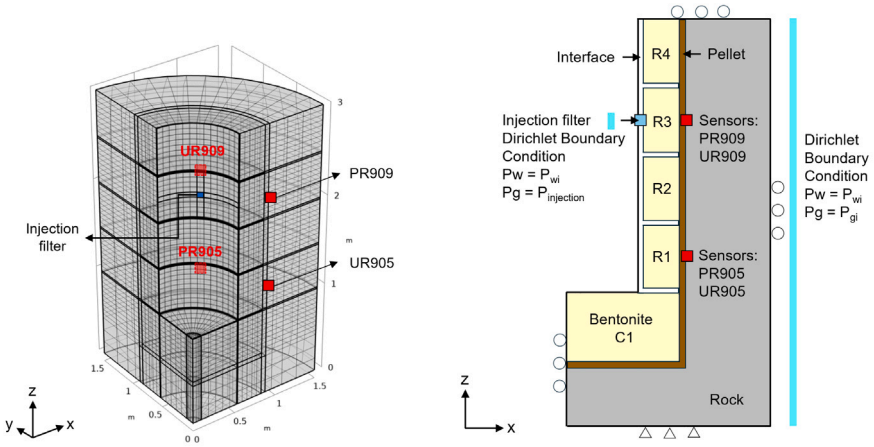

(a) Geometry and mesh configuration (b) Component configuration and boundary condition

Fig. 13. Model configuration.

Table 4
Material properties used in field-scale modeling.

	Meaning	Symbol	Unit	Value for each component				Notes
				Bentonite	Interface[a]	Pellet	Rock	
Mechanical	Average density of porous media	ρ	kg/m^3	1650	1650	1230	2600	Fixed for Bentonite (from Task lead)
	Initial porosity	ϕ_i	–	0.40	0.40	0.56	0.10	Estimated based on ρ
	Initial Young's modulus	E_i	MPa	307	307	226	$700 \cdot 10^2$	Estimated based on ρ
	Biot's coefficient	α	–	0.80	0.80	0.80	0.80	Calibrated
Hydraulic	Initial intrinsic permeability	$\mathbf{k}_{\mathbf{int,i}}$	m^2	$3.40 \cdot 10^{-21}$	$3.40 \cdot 10^{-21}$	$4.23 \cdot 10^{-20}$	$3.73 \cdot 10^{-24}$	Estimated based on ρ[46]
	van Genuchten parameter	m	–	0.45	0.45	0.45	0.45	Calibrated
Damage model	Tensile strength	f_t	MPa	1.20	0.60	1.20	10.0	Calibration parameter
Initial value	Initial pore gas pressure	$p_{g,i}$	MPa	1.87	1.87	1.87	1.87	
	Initial pore water pressure	$p_{w,i}$	MPa	0.31	0.31	0.31	0.31	

[a] In a case that does not consider the interface, the properties of bentonite were applied to the interface.

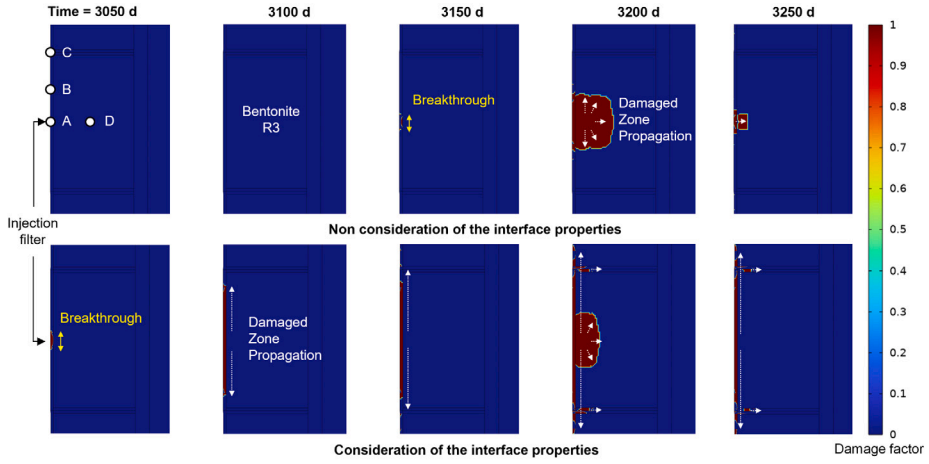

Fig. 14. Comparisons of the damaged zone propagation.

of interface characteristics, pressure transmission along the interfaces (observation points B and C in Fig. 14) occurred more rapidly than through the buffer region (observation point D in Fig. 14), leading to higher stress predictions relative to the case without interface consideration. In contrast, the actual measured data showed minimal changes at all locations compared to the modeling results. This suggests that the injected gas did not significantly reach the interface with the rock and the bentonite blocks where the sensors were placed, instead flowing predominantly interface between the canister and the buffer.

Through this comparison, it was confirmed that the analysis method incorporating interface strength characteristics effectively simulates gas flow along the interfaces. However, the study demonstrated a limitation in predicting damage initiation within the buffer, as it could not adequately manage the phenomenon of excessive pressure transmission into the buffer. This limitation is likely due to the influence of the relative permeability model, which yielded an excessively high gas permeability coefficient, and the insufficient consideration of changes in the water retention curve of the medium, which has vastly different pore structures before and after crack formation. Therefore, future

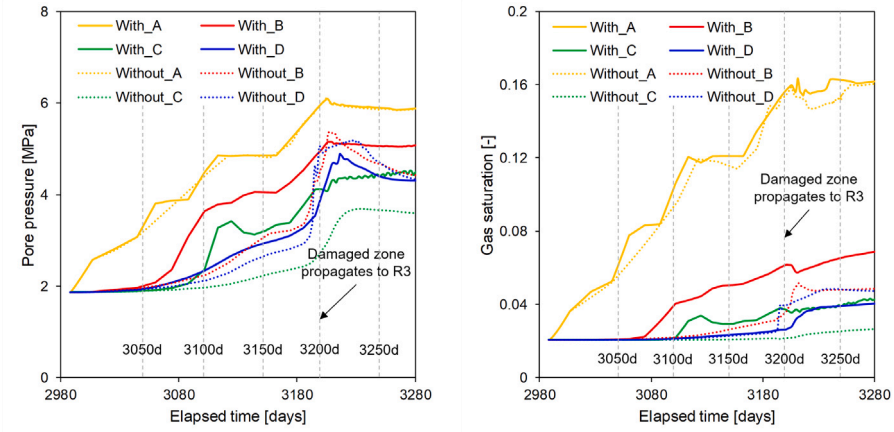

(a) Pore pressure variation with time (b) Gas saturation variation with time

Fig. 15. Pressure and gas saturation at observation points.

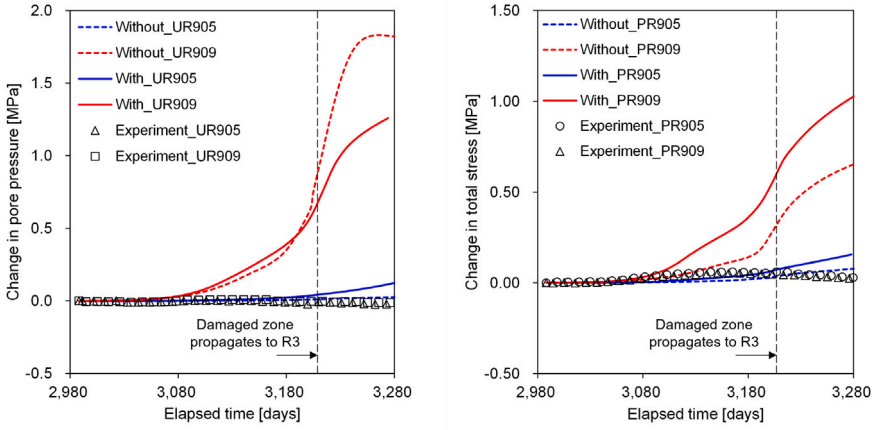

(a) Pore pressure variation (b) Total stress variation

Fig. 16. Comparisons between measured field test data and numerical modeling.

studies should focus on refining the relative permeability model to better capture the impact of changes in the water retention curve on pore pressure transmission following crack formation in the buffer.

5. Conclusions

This study summarizes the research conducted while participating in DECOVALEX-2023 Task B. This study aimed to develop a numerical model for understanding gas migration phenomena in pre-compacted bentonite and test it against a 1D laboratory-scale and a field-scale experiment. Furthermore, modeling of a field-scale test was conducted to investigate the influence of heterogeneity in material properties and the applicability of the developed model to upscaling analysis. The main research contents and results of this study are as follows:

- H^2MD numerical model was developed by combining classical two-phase flow modeling techniques and a damage model. Especially, the damage model was used for simulating a rapid gas flow through the preferential pathway. A damage model was modified to minimize the calibration factor in the original damage model, and we defined the material's tensile strength as the primary damage variable.
- We performed a sensitivity analysis on tensile strength and demonstrated that bentonite's tensile strength directly affects the timing of breakthrough and damage zone propagation.
- A numerical model was tested against a 1D gas injection test simulation. As a result, the main features observed in the gas injection test, (1) rapid changes in stress and pressure due to the breakthrough and (2) an increase in gas flow rate into the bentonite due to the formation of the preferential pathway, were well simulated.
- Additionally, the impact of material property heterogeneity on gas flow pathways was analyzed through field-scale modeling of the Lasgit. The Lasgit analysis encompassed multiple domains, including the interface, bentonite, pellets, and rock, with material heterogeneity incorporated by varying the tensile strength of each material. Consequently, the model that accounted for this heterogeneity accurately simulated the gas flow pathways observed in the actual test.
- Laboratory and field-scale analyses demonstrated that differences in model scale significantly influence the accuracy of damage zone predictions. The laboratory experiment, constrained by limited volume deformation and uniform material properties, underestimated the damaged area due to excessive self-healing within the confined space. In contrast, the field-scale analysis, which incorporated various materials, yielded predictions more consistent with actual test results. These findings confirm the applicability of upscaling approaches that account for material heterogeneity and interface strength characteristics.

The developed model well-captured the gas movement phenomenon in the bentonite. However, the model also has the following limitations:

- Due to the modified relative permeability model, the model overestimates gas movement prior to breakthrough. Additionally, it inadequately accounts for the changes in the damaged area's water retention curves in field-scale tests, resulting in an overestimation of pore pressure transmission. Consequently, this leads to an excessive prediction of the damaged area within the buffer material.
- The damage model employed in this study, which does not account for compressive failure, predicted a broad, rather than a discontinuous and narrow, damaged area and overestimated that the damaged area would recover completely after self-healing.

These findings provide valuable insights into the impact of bentonite's tensile strength and the interactions between components of the disposal system on gas migration pathways within the repository. Consequently, the results of this study are expected to inform the development of numerical models for the design and long-term stability analysis of deep geological repositories.

CRediT authorship contribution statement

Jung-Tae Kim: Writing – review & editing, Writing – original draft, Visualization, Validation, Methodology, Formal analysis, Data curation, Conceptualization. **Changsoo Lee:** Writing – review & editing, Validation, Supervision, Methodology, Conceptualization. **Minhyeong Lee:** Writing – review & editing, Data curation. **Jin-Seop Kim:** Project administration. **E. Tamayo-Mas:** Writing – review & editing. **J.F. Harrington:** Writing – review & editing, Project administration.

Declaration of competing interest

The authors declare that they have no known competing financial interests or personal relationships that could have appeared to influence the work reported in this paper.

Acknowledgments

The authors appreciate and thank the DECOVALEX-2023 Funding Organisations Andra, BASE, BGE, BGR, CAS, CNSC, COVRA, US DOE, ENRESA, ENSI, JAEA, KAERI, NWMO, RWM, SÚRAO, SSM and Taipower for their financial and technical support of the work described in this paper. The statements made in the paper are, however, solely those of the authors and do not necessarily reflect those of the Funding Organisations. This research was also supported by the Institute for Korea Spent Nuclear Fuel (iKSNF) and National Research Foundation of Korea (NRF) grant funded by the Korea government (Ministry of Science and ICT, MSIT) (2021M2E1A1085193).

Data availability

Data will be made available on request.

References

1. Rodwell W, Harris A, Horseman S, Lalieux P, Müller W, Ortiz Amaya L, Pruess K. Gas migration and two-phase flow through engineered and geological barriers for a deep repository for radioactive waste. *EUR (Luxembourg)*. 1999.
2. Abdi H, Labrie D, Nguyen T, Barnichon J-D, Su G, Evgin E, Simon R, Fall M. Laboratory investigation on the mechanical behaviour of tournemire argillite. *Can Geotech J*. 2015;52(3):268–282.
3. Liu J-F, Song Y, Skoczylas F, Liu J. Gas migration through water-saturated bentonite–sand mixtures, COx argillite, and their interfaces. *Can Geotech J*. 2015;53(1):60–71.
4. Yoon S, Lee G-J, An S. Pressure evaluation of a gap space in the engineered barrier system in a high-level radioactive waste repository. *Case Stud Therm Eng*. 2023;50:103458.
5. Komine H. Simplified evaluation for swelling characteristics of bentonites. *Eng Geol*. 2004;71(3–4):265–279.
6. Villar MV, Lloret A. Influence of temperature on the hydro-mechanical behaviour of a compacted bentonite. *Appl Clay Sci*. 2004;26(1–4):337–350.
7. Sellin P, Leupin OX. The use of clay as an engineered barrier in radioactive-waste management a review. *Clays Clay Miner*. 2013;61:477–498.
8. Xu L, Ye W, Ye B, Chen B, Chen Y, Cui Y-J. Investigation on gas migration in saturated materials with low permeability. *Eng Geol*. 2015;197:94–102.
9. Lee G-J, Yoon S, Kim B-J. Prediction model for saturated hydraulic conductivity of bentonite buffer materials for an engineered-barrier system in a high-level radioactive waste repository. *J Nucl Fuel Cycle Waste Technol*. 2023;21(2):225–234.
10. Weetjens E, Sillen X. Gas generation and migration in the near field of a supercontainer-based disposal system for vitrified high-level radioactive waste. In: *Proc. 11th Int. High-Level Radioactive Waste Management Conf. (IHLRWM), Las Vegas, Nevada*. 2006.
11. Marschall P, Horseman S, Gimmi T. Characterisation of gas transport properties of the Opalinus Clay, a potential host rock formation for radioactive waste disposal. *Oil Gas Sci Technol*. 2005;60(1):121–139.
12. Ye W-M, Xu L, Chen B, Chen Y-G, Ye B, Cui Y-J. An approach based on two-phase flow phenomenon for modeling gas migration in saturated compacted bentonite. *Eng Geol*. 2014;169:124–132.
13. Yang J, Fall M. Coupled hydro-mechanical modelling of dilatancy controlled gas flow and gas induced fracturing in saturated claystone. *Int J Rock Mech Min Sci*. 2021;138:104584.
14. Graham C, Harrington J, Cuss R, Sellin P. Gas migration experiments in bentonite: Implications for numerical modelling. *Mineral Mag*. 2012;76(8):3279–3292.
15. Guo G, Fall M. Advances in modelling of hydro-mechanical processes in gas migration within saturated bentonite: A state-of-art review. *Eng Geol*. 2021;287:106123.
16. Harrington J, Horseman S. *Gas Migration in KBS-3 Buffer Bentonite. Sensitivity of Test Parameters to Experimental Boundary Conditions*. Tech. Rep.; Swedish Nuclear Fuel and Waste Management Co.; 2003.
17. Harrington JF, Graham CC, Cuss RJ, Norris S. Gas network development in a precompacted bentonite experiment: Evidence of generation and evolution. *Appl Clay Sci*. 2017;147:80–89.
18. Cuss RJ, Harrington JF, Noy DJ, Wikman A, Sellin P. Large scale gas injection test (Lasgit): Results from two gas injection tests. *Phys Chem Earth A/B/C*. 2011;36(17–18):1729–1742.
19. Cuss R, Harrington J, Noy D, Graham C, Sellin P. Evidence of localised gas propagation pathways in a field-scale bentonite engineered barrier system; results from three gas injection tests in the large scale gas injection test (Lasgit). *Appl Clay Sci*. 2014;102:81–92.
20. Senger R, Lanyon B, Marschall P, Vomvoris S, Fujiwara A. Numerical modeling of the gas migration test at the Grimsel test site (Switzerland). *Nucl Technol*. 2008;164(2):155–168.
21. Xu W, Shao H, Hesser J, Wang W, Schuster K, Kolditz O. Coupled multiphase flow and elasto-plastic modelling of in-situ gas injection experiments in saturated claystone (Mont Terri Rock Laboratory). *Eng Geol*. 2013;157:55–68.
22. Tamayo-Mas E, Harrington J, Shao H, Dagher E, Lee J, Kim K, Rutqvist J, Lai S-H, Chittenden N, Wang Y, et al Numerical modelling of gas flow in a compact clay barrier for DECOVALEX-2019. In: *ARMA International Discrete Fracture Network Engineering Conference*. ARMA; 2018:D033S015R001.
23. Tamayo-Mas E, Harrington J, Brüning T, Shao H, Dagher E, Lee J, Kim K, Rutqvist J, Kolditz O, Lai S, et al Modelling advective gas flow in compact bentonite: Lessons learnt from different numerical approaches. *Int J Rock Mech Min Sci*. 2021;139:104580.
24. Nguyen T, Le A. Simultaneous gas and water flow in a damage-susceptible bedded argillaceous rock. *Can Geotech J*. 2015;52(1):18–32.
25. Fall M, Nasir O, Nguyen T. A coupled hydro-mechanical model for simulation of gas migration in host sedimentary rocks for nuclear waste repositories. *Eng Geol*. 2014;176:24–44.
26. Dagher E, Nguyen T, Infante Sedano J. Development of a mathematical model for gas migration (two-phase flow) in natural and engineered barriers for radioactive waste disposal. *Geol Soc Lond Special Publ*. 2019;482(1):115–148.
27. Tamayo-Mas E, Harrington J, Damians I, Olivella S, Radeisen E, Rutqvist J, Wang Y. Advective gas flow in bentonite: Development and comparison of enhanced multi-phase numerical approaches. *Geomech Energy Environ*. 2024;37:100528.
28. Xue Y, Dang F, Shi F, Li R, Cao Z. Evaluation of gas migration and rock damage characteristics for underground nuclear waste storage based on a coupled model. *Sci Technol Nucl Install*. 2018;2018(1):2973279.
29. Dagher EE, Nguyen TS, Sedano JÁI. Investigating models to represent gas transport in a swelling geomaterial. *Int J Rock Mech Min Sci*. 2021;137:104457.
30. Yang J, Fall M. A two-scale time dependent damage model for preferential gas flow in clayey rock materials. *Mech Mater*. 2021;158:103853.
31. Daniels K, Harrington J. The response of compact bentonite during a 1-D gas flow test. 2017.
32. Horseman S, Harrington J, Sellin P. Gas migration in clay barriers. *Eng Geol*. 1999;54(1–2):139–149.

33. Olivella S, Alonso E. Gas flow through clay barriers. *Géotechnique*. 2008;58(3):157–176.
34. Waste R. Effects of post-disposal gas generation in a repository for low-and intermediate-level waste sited in the Opalinus Clay of Northern Switzerland. 2008.
35. Rutqvist J, Ijiri Y, Yamamoto H. Implementation of the Barcelona basic model into TOUGH–FLAC for simulations of the geomechanical behavior of unsaturated soils. *Comput Geosci*. 2011;37(6):751–762.
36. Van Genuchten MT. A closed-form equation for predicting the hydraulic conductivity of unsaturated soils. *Soil Sci Soc Am J*. 1980;44(5):892–898.
37. Mualem Y. A new model for predicting the hydraulic conductivity of unsaturated porous media. *Water Resour Res*. 1976;12(3):513–522.
38. Tang CA, Tham LG, Lee P, Yang T, Li L. Coupled analysis of flow, stress and damage (FSD) in rock failure. *Int J Rock Mech Min Sci*. 2002;39(4):477–489.
39. Wang J, Elsworth D, Wu Y, Liu J, Zhu W, Liu Y. The influence of fracturing fluids on fracturing processes: A comparison between water, oil and SC-CO 2. *Rock Mech Rock Eng*. 2018;51:299–313.
40. Cui G, Wei J, Feng X-T, Liu J, Elsworth D, Chen T, Xiong W. Preliminary study on the feasibility of co-exploitation of coal and uranium. *Int J Rock Mech Min Sci*. 2019;123:104098.
41. Meschke G, Grasberger S. Numerical modeling of coupled hygromechanical degradation of cementitious materials. *J Eng Mech*. 2003;129(4):383–392.
42. Villar M. MX-80 bentonite. Thermal-hydro-mechanical characterisation performed at CIEMAT in the context of the prototype project. CIEMAT-1053. 2005.
43. Lee J, Lee C, Kim GY. Numerical modelling of one dimensional gas injection experiment using mechanical damage model: Decovalex-2019 task a stage 1a. *Tunn Undergr Space*. 2019;29(4):262–279.
44. Tamayo-Mas E, Harrington J, Brüning T, Kolditz O, Shao H, Dagher E, Lee C, Lee J, Kim K, Lai S, et al *Decovalex-2019 (Task A Final Report)*. Tech. Rep.; Berkeley, CA (United States): Lawrence Berkeley National Lab. (LBNL); 2020.
45. Villar MV, Carbonell B, Martín PL, Gutiérrez-Álvarez C. The role of interfaces in the bentonite barrier of a nuclear waste repository on gas transport. *Eng Geol*. 2021;286:106087.
46. Park S, Yoon S, Kwon S, Kim G-Y. A prediction of saturated hydraulic conductivity for compacted bentonite buffer in a high-level radioactive waste disposal system. *J Nucl Fuel Cycle Waste Technol (JNFCWT)*. 2020;18(2):133–141.